

**Cell Reports, Volume 33**

**Supplemental Information**

**ARID1A Mutations Promote P300-Dependent  
Endometrial Invasion through  
Super-Enhancer Hyperacetylation**

**Mike R. Wilson, Jake J. Reske, Jeanne Holladay, Subechhya Neupane, Julie Ngo, Nina Cuthrell, Marc Wegener, Mary Rhodes, Marie Adams, Rachael Sheridan, Galen Hostetter, Fahad T. Alotaibi, Paul J. Yong, Michael S. Anglesio, Bruce A. Lessey, Richard E. Leach, Jose M. Teixeira, Stacey A. Missmer, Asgerally T. Fazleabas, and Ronald L. Chandler**

**Figure S1**

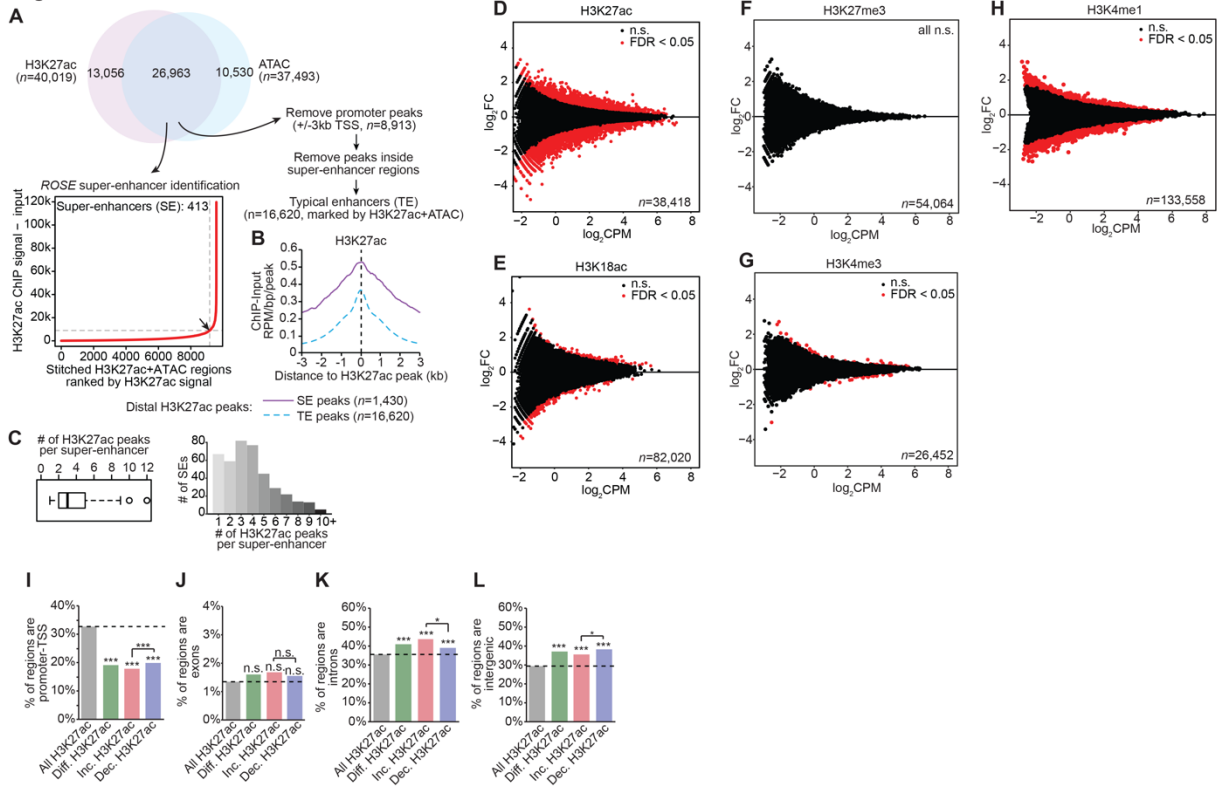


**Figure S1. Enhancer classification and additional differential histone modification analysis, related to Figures 1 and 2.**

(A) Identification of super-enhancers (SE) and typical enhancers (TE) using *ROSE* identification. 26,963 H3K27ac regions with overlapping accessibility (ATAC) were used as input for *ROSE*, leading to identification of 413 active SE. TE were defined by filtering these SE regions along with any overlapping gene promoters from the remaining H3K27ac peaks.

(B) Meta peak plots for H3K27ac at distal peaks within SE or TE, centered on the H3K27ac peak. y-axis is signal as ChIP – Input reads per million (RPM) per bp per peak.

(C) Number of H3K27ac peaks per SE depicted as a boxplot in the style of Tukey (left) or a histogram (right). The median number of peaks per SE is 3.

(D-H) Differential (D) H3K27ac, (E) H3K18ac, (F) H3K27me3, (G) H3K4me3 and (H) H3K4me1 ChIP-seq following ARID1A loss. MA plots display differential abundance with significant sites (FDR < 0.05) highlighted in red. x-axis is signal abundance quantified as log<sub>2</sub> counts per million (log<sub>2</sub>CPM), and y-axis is the log<sub>2</sub> fold change (log<sub>2</sub>FC) difference of shARID1A vs. control conditions (n = 2 ChIP replicates per condition).

(I-L) Genomic feature enrichment for sites with all differential, increasing or decreasing H3K27ac, compared to all tested H3K27ac regions, which are found in (I) promoters, (J) exons, (K) introns, or (L) intergenic regions. Statistic is hypergeometric enrichment and pairwise two-tailed Fisher’s exact test.

Figure S2

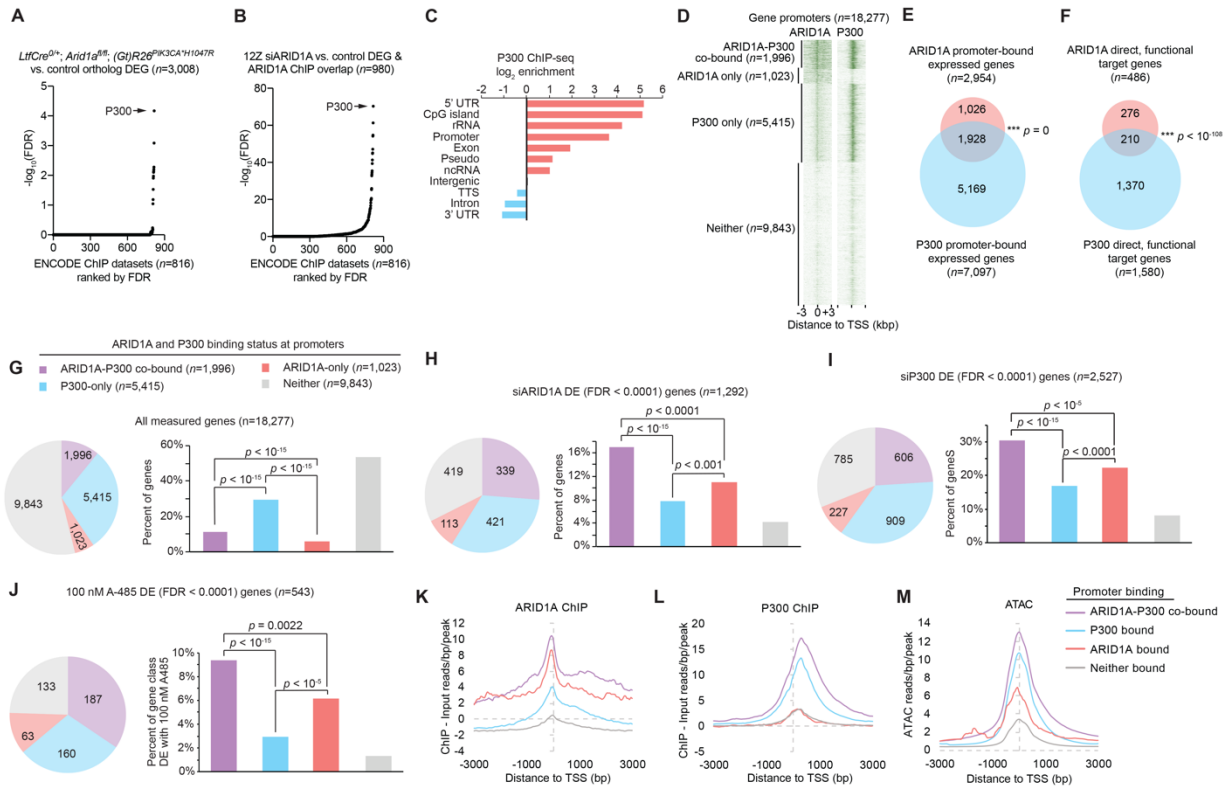


**Figure S2. ARID1A and P300 co-regulation of promoters and gene expression, related to Figure 3.**

(A and B) Differentially expressed genes from (A) *LtfCre<sup>0/+</sup>; Arid1a<sup>fl/fl</sup>; (Gt)R26<sup>fl/fl</sup>; Ptk3ca<sup>H1047R</sup>* mice compared to control (FDR < 0.05,  $n = 3,008$  human orthologs) or (B) genes bound by ARID1A and differentially expressed upon ARID1A loss in 12Z cells (FDR < 0.05,  $n = 980$ ) were analyzed using the Enrichr webtool for overlap with co-factor binding from ENCODE database. Significance ( $\log_{10}(\text{FDR})$ , y-axis) of overlapping datasets, ranked by FDR-value (x-axis). P300 is the most significant co-factor in both datasets (arrow).

(C) Enrichment for significant genomic features among P300 ChIP peaks, ranked by  $p$ -value. Enrichment ratio is calculated by bp of feature in ChIP peak set compared to background genome.

(D) Heatmap of ARID1A and P300 ChIP-seq signal at 18,277 gene promoters, arranged into groups based on significant binding of ARID1A, P300, both ARID1A and P300, or neither.

(E) Euler diagram of overlap between expressed gene promoters bound by ARID1A ( $n = 2,954$ ) and P300 ( $n = 7,097$ ). Statistic is hypergeometric enrichment.

(F) Euler diagram of overlap between direct, functional target genes of ARID1A ( $n = 486$ ) and P300 ( $n = 1,580$ ). Direct, functional target genes were defined by ChIP promoter binding and which knockdown (by siARID1A or siP300) led to a significant change in gene expression. Statistic is hypergeometric enrichment.

(G-J) Percent of genes bound by ARID1A, EP300 or both among all genes (G) or genes which were differentially expressed following knockdown of ARID1A (H), EP300 (I) or 100 nM A-485 treatment (J). Statistic is two-tailed Fisher's exact test.

(K-M) Meta peak profile of ARID1A binding (K), P300 binding (L) or chromatin accessibility (ATAC) (M) at promoters with ARID1A binding, P300 binding, both, or neither. y-axis is ChIP - Input reads per bp per peak (K, L) or ATAC reads per bp per peak (M).

**Figure S3**

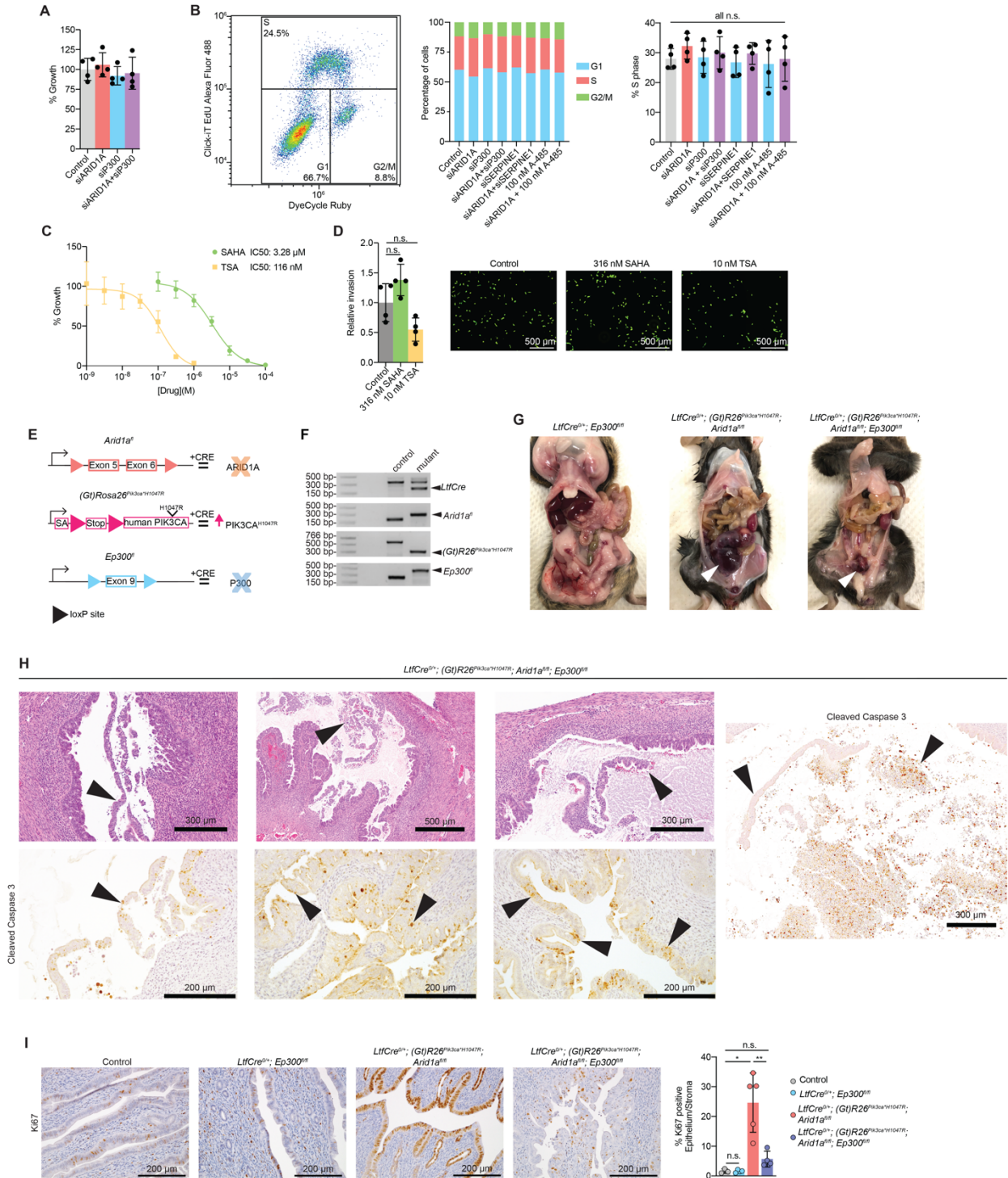


**Figure S3. Additional characterization of P300-deficient phenotypes, related to Figure 4.**

(A) Measurement of 12Z cell growth 72 hours post-transfection. No significant differences were observed (unpaired, two-tailed *t*-test). Mean  $\pm$  S.D.,  $n = 4$ .

(B) Cell cycle analysis cells treated with siRNA co-treatment or A-485 treatment. Analysis was performed 72 hrs after transfection and 48 hrs after drug treatment. EdU incorporation and DyeCycle Ruby staining were measured by flow cytometry and used to determine cell cycle. No significant differences in S-phase (EdU) incorporation as a marker of proliferation were observed (right plot). Statistic is unpaired, two-tailed Mann-Whitney U test.

(C) Measurement of 12Z cell growth following 72 hours SAHA or TSA treatment. Cells were stained with calcein-AM for 1 hour prior to imaging. Data represents normalized fluorescence value relative to control (vehicle). Mean  $\pm$  S.D.,  $n = 4$ .

(D) Invasion of 12Z cells following treatment with 316 nM SAHA or 10 nM TSA. Representative images of calcein-AM stained cells and total invaded cell numbers are shown (scale bar = 500  $\mu\text{m}$ ). No significant differences were observed (unpaired, two-tailed  $t$ -test). Mean  $\pm$  S.D.,  $n = 4$ .

(E) Illustration of mutant alleles used in this study.

(F) PCR genotyping results to detect *LtfCre*<sup>0/+</sup>, *(Gt)R26Pik3ca*<sup>\*H1047R</sup>, *Arid1a*<sup>fl</sup>, and *Ep300*<sup>fl</sup>.

(G) Representative gross images of mouse uterus and uterine tumors. White arrowheads indicate tumors. *LtfCre*<sup>0/+</sup>; *(Gt)R26Pik3ca*<sup>\*H1047R</sup>; *Arid1a*<sup>fl/fl</sup> ( $n = 16$ ) and *LtfCre*<sup>0/+</sup>; *(Gt)R26Pik3ca*<sup>\*H1047R</sup>; *Arid1a*<sup>fl/fl</sup>; *Ep300*<sup>fl/fl</sup> mice ( $n = 12$ ) were sacrificed at the point of vaginal bleeding. *LtfCre*<sup>0/+</sup>; *Ep300*<sup>fl/fl</sup> mice were aged out to 187 days ( $n = 6$ ).

(H) Additional histology and IHC staining for Cleaved-Caspase 3 in *LtfCre*<sup>0/+</sup>; *(Gt)R26Pik3ca*<sup>\*H1047R</sup>; *Arid1a*<sup>fl/fl</sup>; *Ep300*<sup>fl/fl</sup> mouse endometrium. Arrowheads indicate endometrial epithelium. Scale bar is indicated size between 200  $\mu\text{m}$  and 500  $\mu\text{m}$ .

(I) Ki67 IHC staining and quantification. Representative images of Ki67 staining in control, *LtfCre*<sup>0/+</sup>, *Ep300*<sup>fl/fl</sup>; *LtfCre*<sup>0/+</sup>; *(Gt)R26Pik3ca*<sup>\*H1047R</sup>, *Arid1a*<sup>fl/fl</sup> and *LtfCre*<sup>0/+</sup>; *(Gt)R26Pik3ca*<sup>\*H1047R</sup>, *Arid1a*<sup>fl/fl</sup>, *Ep300*<sup>fl/fl</sup> mice. Number of Ki67+ cells and total cells were counted in the epithelium and stroma and plotted as a ratio of % positive epithelia/stroma. Mean  $\pm$  S.D.,  $n = 3-5$  mice, unpaired, two-tailed  $t$ -test, \*\*\*  $p < 0.001$ .

**Figure S4**

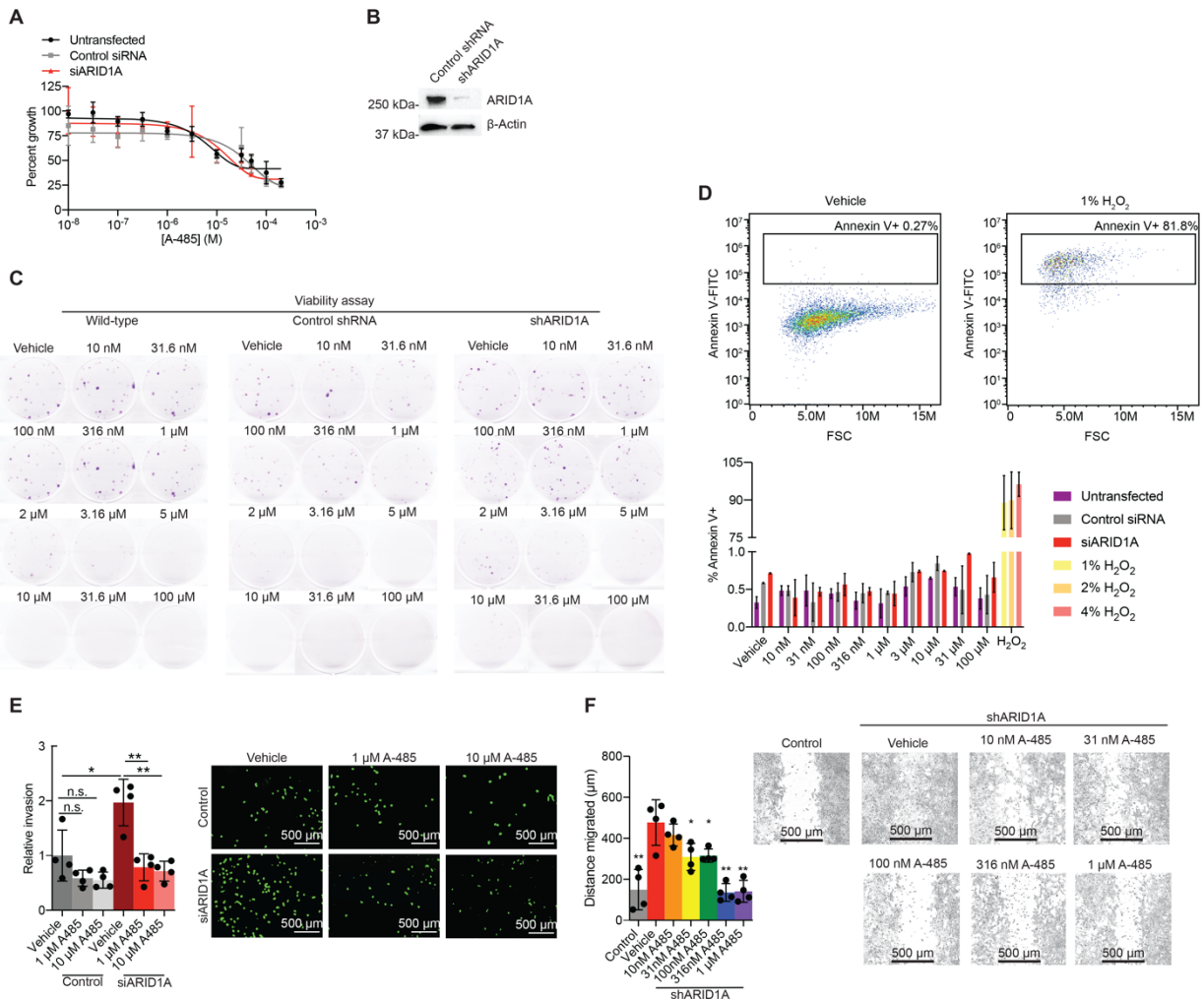


**Figure S4. Phenotypic characterization of cells following A-485 treatment, related to Figure 4.**

(A) Measurement of 12Z cell growth following 72 hours of A-485 treatment. Data represents normalized fluorescence value relative to vehicle control. Mean ± S.D.,  $n = 4$ .

(B) Western blot depicting ARID1A knockdown in shARID1A stable cell line. β-Actin was used as a loading control.

(C) Viability assay for cells treated with A-485. Statistical analysis presented in Figure 4G.

(D) Annexin-V staining of cells treated with A-485 following siRNA treatment. Cells were treated with A-485 for 24 hours. Annexin-V-FITC signal was measured by flow cytometry, and H<sub>2</sub>O<sub>2</sub> treatment was used as a positive control. Histogram represents percentage of Annexin-V+ cells in each sample. Mean ± S.D.,  $n = 2$ .

(E) Invasion of 12Z cells following treatment with non-targeting siRNA or siARID1A and A-485 treatment from 1 μM to 10 μM. Representative images of calcein-AM stained cells and total invaded cell numbers are shown (scale bar = 500 μm). Mean ± S.D.,  $n = 4$ . Unpaired, two-tailed  $t$ -test.

(F) Migration assay of 12Z cells following treatment with shARID1A and A-485 treatment from 10 nM to 1 μM. Images are representative of cells 24 hrs following removal of insert (scale bar = 500 μm). Migration distance represents the average difference distance across each migration front from 0 to 24 hrs. Mean ± S.D.,  $n = 4$ .

Unpaired, two-tailed  $t$ -tests were performed in comparison to the shARID1A + vehicle condition.

\*  $p < 0.05$ , \*\*  $p < 0.01$ .



**Figure S5**

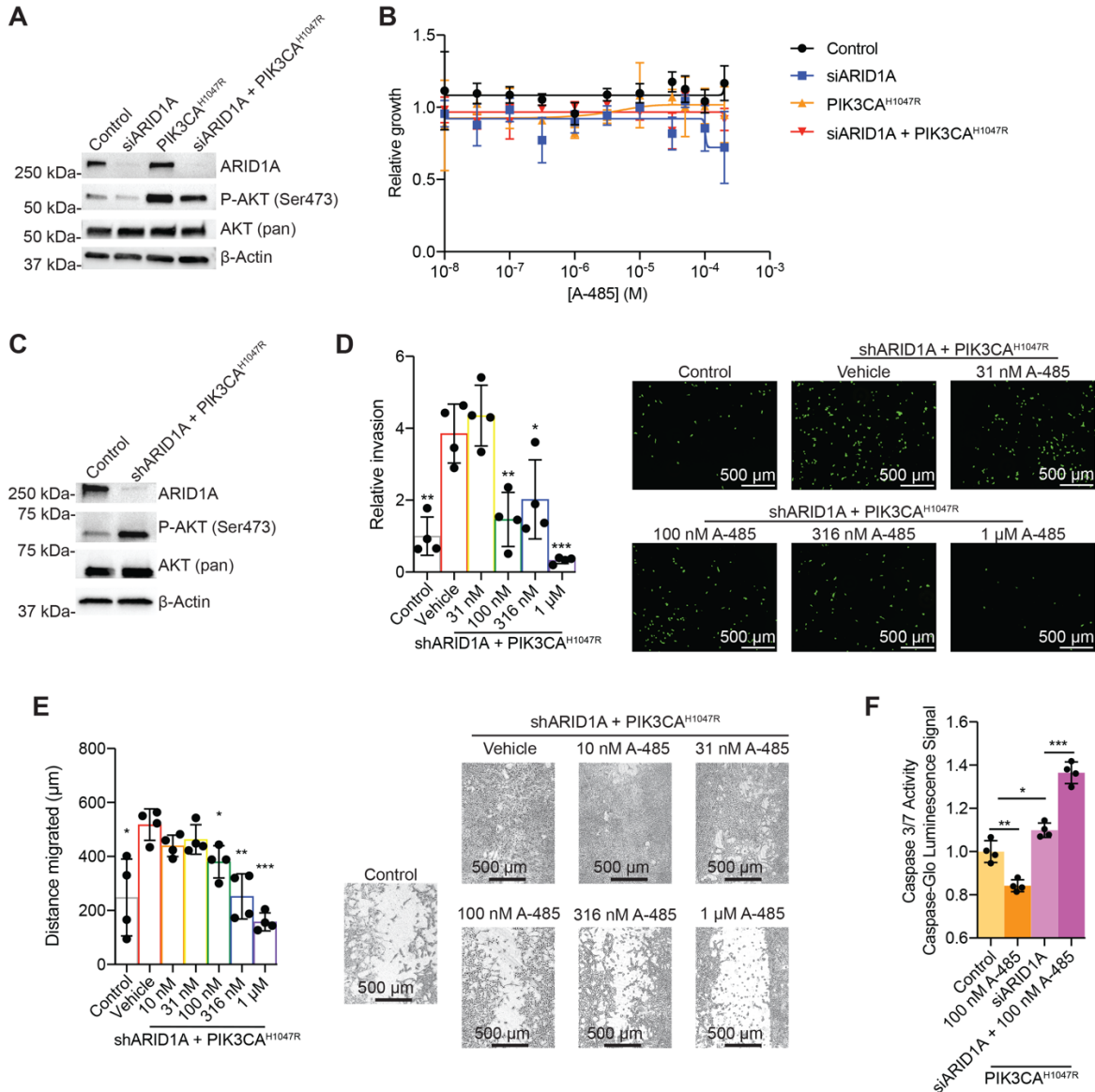


**Figure S5. Effects of A-485 treatment on ARID1A and PIK3CA double-mutant 12Z cells, related to Figure 4.**

(A) Western blot of ARID1A, β-Actin, AKT, P-AKT following co-transfection of non-targeting siRNA (control) + empty vector, siARID1A + empty vector, non-targeting siRNA + PIK3CA<sup>H1047R</sup> plasmid or siARID1A + PIK3CA<sup>H1047R</sup> plasmid.

(B) Measurement of 12Z cell growth following 48 hours of A-485 treatment. Data represents normalized fluorescence value relative to vehicle control. Mean ± S.D., *n* = 4.

(C) Western blot of ARID1A, β-Actin, AKT, P-AKT following co-transfection of non-targeting shRNA (control) + empty vector or shARID1A + PIK3CA<sup>H1047R</sup> plasmid.

(D) Invasion of 12Z cells following treatment with shARID1A, PIK3CA<sup>H1047R</sup> plasmid and A-485 treatment from 31 nM to 1 μM. Representative images of calcein-AM stained cells and total invaded cell numbers are shown (scale bar = 500 μm). Mean ± S.D., *n* = 4. Unpaired, two-tailed *t*-tests were performed in comparison to the shARID1A, PIK3CA<sup>H1047R</sup> + vehicle condition.

(E) Migration assay of 12Z cells following treatment with shARID1A, PIK3CA<sup>H1047R</sup> plasmid and A-485 treatment from 10 nM to 1 μM. Images are representative of cells 24 hrs following removal of insert (scale bar = 500 μm). Migration distance represents the average difference distance across each migration front from 0 to 24 hrs. Mean ±

S.D.,  $n = 4$ . Unpaired, two-tailed  $t$ -tests were performed in comparison to the shARID1A, PIK3CA<sup>H1047R</sup> + vehicle condition.

(F) Caspase-Glo assay of 12Z cells in suspension following treatment with shARID1A and PIK3CA<sup>H1047R</sup> plasmid.

Mean  $\pm$  S.D.,  $n = 4$ , unpaired, two-tailed  $t$ -test.

\*  $p < 0.05$ , \*\*  $p < 0.01$ , \*\*\*  $p < 0.001$ .



## Figure S6

A

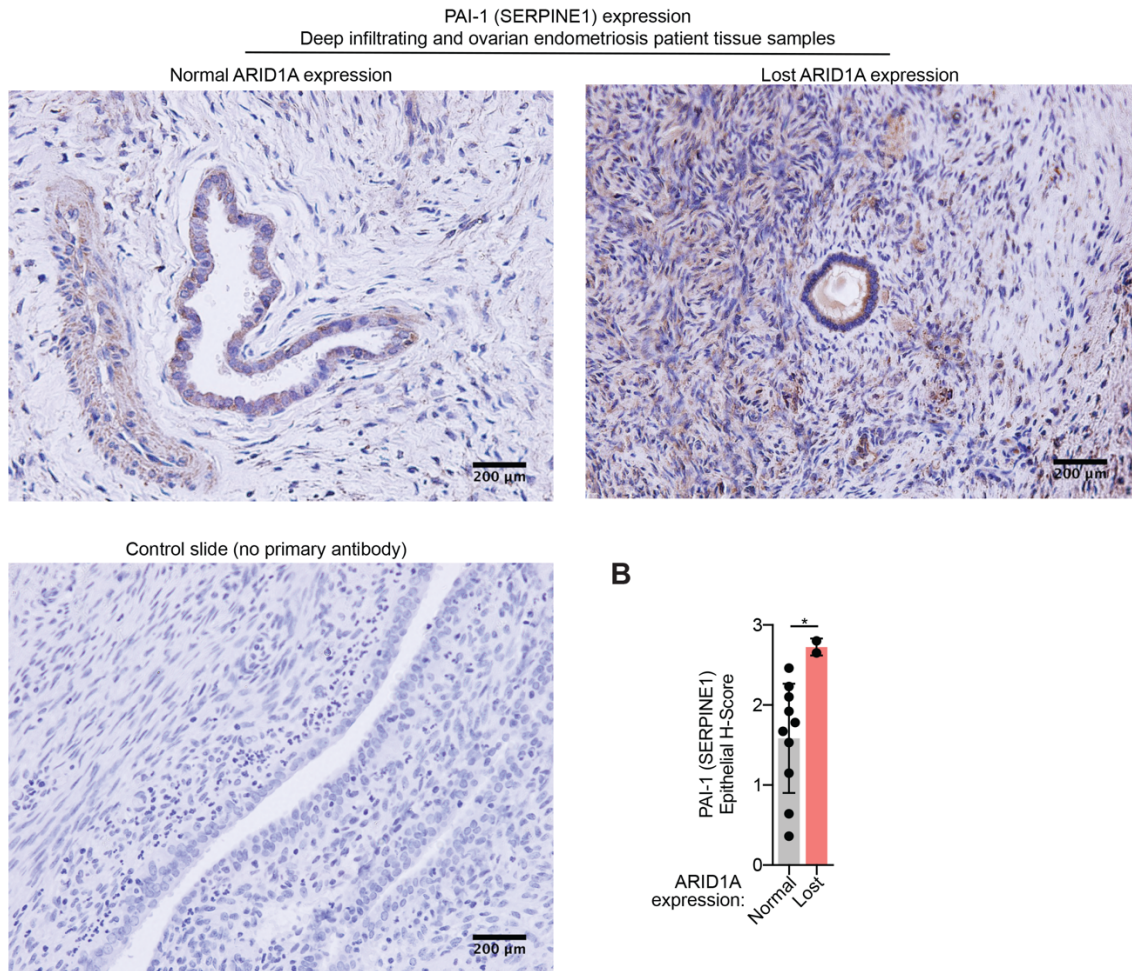


**Figure S6. SERPINE1 immunohistochemical staining in endometriosis patient samples, related to Figure 7.** (A) IHC staining for SERPINE1/PAI-1 in human deep infiltrating and ovarian endometriosis patient tissues samples. Scale bars = 200  $\mu$ m.

(B) IHC quantification of SERPINE/PAI-1 as epithelial H-score, comparing ARID1A-expressing ( $n = 10$ ) vs. ARID1A-lost ( $n = 2$ ) lesions. Statistic is unpaired, two-tailed  $t$ -test.

\*  $p < 0.05$

**Figure S7**

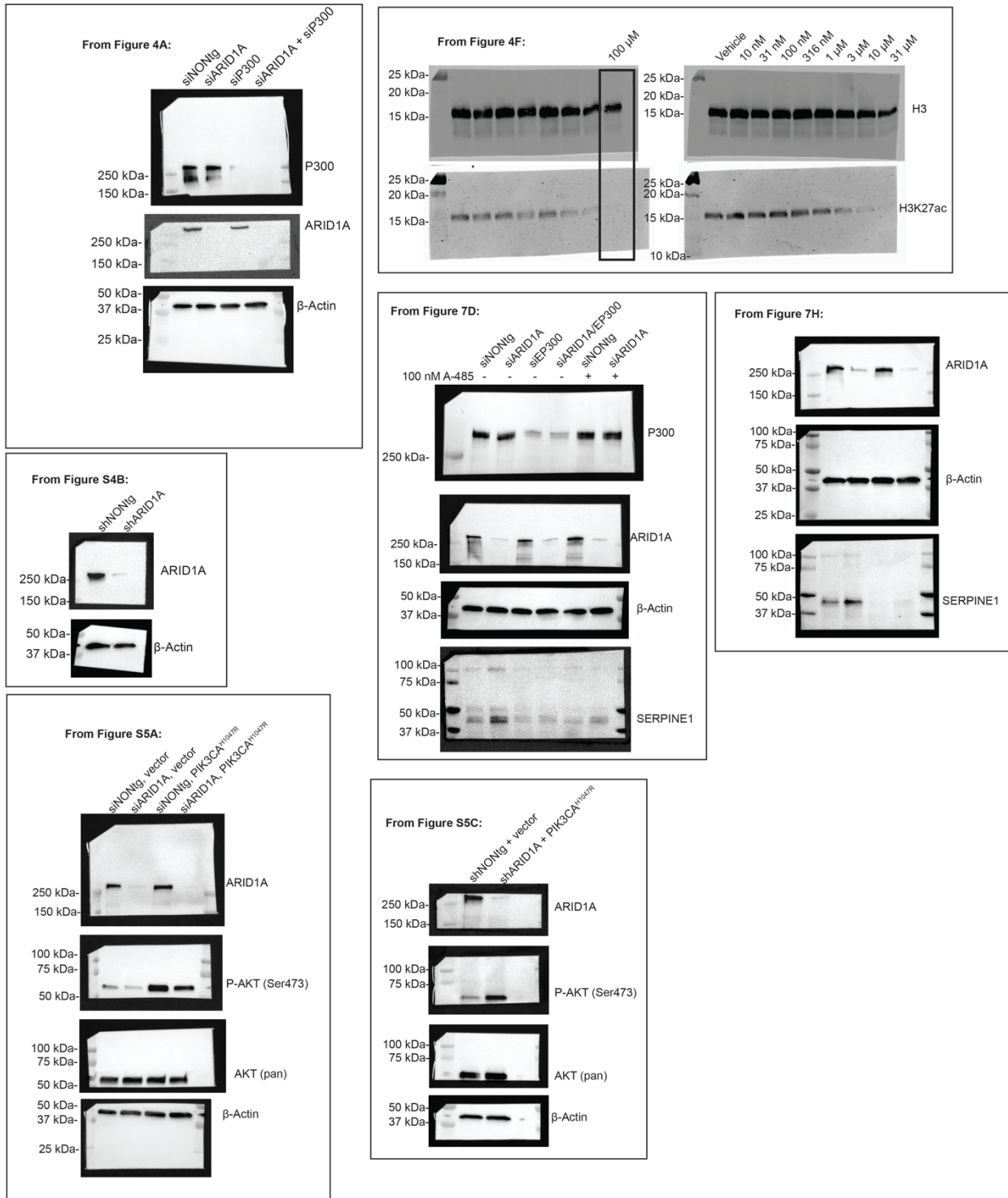


**Figure S7. Uncropped western blots, related to Figures 4 and 7.**